

On-Robot Policy Learning with $O(2)$ -Equivariant SAC

Dian Wang

Mingxi Jia

Xupeng Zhu

Robin Walters

Robert Platt

Khoury College of Computer Sciences
Northeastern University
Boston, MA 02115, USA

{wang.dian, jia.ming, zhu.xup, r.walters, r.platt}@northeastern.edu

Abstract—Recently, equivariant neural network models have been shown to be useful in improving sample efficiency for tasks in computer vision and reinforcement learning. This paper explores this idea in the context of on-robot policy learning where a policy must be learned entirely on a physical robotic system without reference to a model, a simulator, or an offline dataset. We focus on applications of $SO(2)$ -Equivariant SAC to robotic manipulation and explore a number of variations of the algorithm. Ultimately, we demonstrate the ability to learn several non-trivial manipulation tasks completely through on-robot experiences in less than an hour or two of wall clock time.

I. INTRODUCTION

The dream of robotic learning is to develop algorithms that can enable a robot to learn or improve new behaviors online in the physical world. Unfortunately, reinforcement learning algorithms are generally not sufficiently sample efficient to support this goal. As a result, researchers are typically stuck between two less-than-ideal options: 1) to learn in simulation and then transfer policy knowledge onto a physical robot [20, 33]; 2) to spend hundreds of hours learning through interaction on a physical robot [15, 10]. Neither of these options is ideal. If we learn policies in simulation, there is a risk of significantly degraded performance when running those policies on a real robot due to the sim2real domain gap. If we learn policies via real-robot experience, then not only do we need to spend a long time running a physical robot, but it becomes difficult to learn on-policy and performance is again compromised. In this paper, we explore the degree to which a new equivariant RL algorithm known as $SO(2)$ -Equivariant SAC [26] can facilitate on-robot learning. The equivariant model used by this algorithm incorporates a strong prior that can significantly improve the sample efficiency of the algorithm for visual robot learning. Here, we experimentally evaluate the effect of various algorithmic choices on sample efficiency and demonstrate that the resulting algorithm is an attractive choice for on-robot learning.

On-robot learning is challenging because it is expensive to acquire samples. A typical environmental step on a physical robot system is often at least one order of magnitude more time-consuming than one environmental step in the simulation. Traditional approaches often require hundreds of robot hours to train a policy [19, 10]. Recently, several researchers have demonstrated that various forms of data augmentation

and contrastive learning can improve sample efficiency in RL [13, 12, 14]. Zhan et al. [32] applied these ideas to robotic manipulation and demonstrated that it was possible to learn simple manipulation tasks on-line with a physical robot in about an hour. Unfortunately, that system was unable to control the orientation of the gripper – only gripper position and aperture were under control by the policy.

In contrast to data augmentation and contrastive learning, equivariant neural networks [3, 4] enforce symmetry directly in the structure of the neural network. This can improve sample efficiency when learning an invariant or equivariant function and it has been shown to be helpful for visual robot policy learning because many robotics tasks contain some level of rotational symmetry [25, 26]. However, there has been no prior work to our knowledge that evaluates the potential of equivariant reinforcement learning in the context of physical on-robot learning.

In this work, we explore on-robot learning using a recently proposed equivariant RL algorithm known as $SO(2)$ -Equivariant SAC [26]. We make two contributions. First, we extend the $SO(2)$ symmetry of $SO(2)$ -Equivariant SAC to $O(2)$, and experimentally evaluate the effect of a number of algorithmic choices on the sample efficiency of $O(2)$ -Equivariant SAC in the context of four challenging robotic manipulation problems. Second, we demonstrate that the resulting algorithm can learn good policies from scratch on a physical robot in between 45 minutes and two hours.

II. RELATED WORK

A. Equivariant Learning

Equivariant neural networks were first introduced in G-Convolution [3] and Steerable CNNs [4] to improve the sample efficiency of traditional convolutional neural networks by injecting symmetries in the structure of the neural network. Weiler and Cesa [28] proposed a framework for implementing general $E(2)$ Steerable CNNs. Recent work showed encouraging results for applying equivariant networks in various computer vision [1, 6] and dynamics [27, 23] tasks. They have also been applied to deep RL [16, 22] and robotic manipulation [25, 26] with good results. However, to our knowledge, equivariant RL methods have never been explored in the context of on-robot learning.

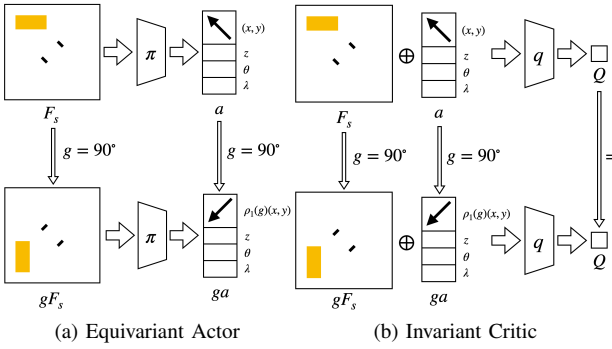


Fig. 1. Illustration of the Equivariant SAC. (a): the equivariant actor’s output action rotates as the input state rotates. (b): the invariant critic’s output doesn’t change when the input state and action are rotated simultaneously.

B. On-Robot Learning

The most common approach to robotic policy learning is to train in simulation and then transfer to a real world application [20, 33, 8, 24, 2]. Nevertheless, there have been several efforts to develop methods that enable an agent to learn a policy directly on a physical robotic system. Gu et al. [7] trained manipulation skills in fixed environments with multiple physical robot workers. Singh et al. [21] developed a method that learned manipulation skills within 1-4 hours in the real world but required a user to respond to queries for labels. Kalashnikov et al. [10] trained a grasping policy with seven robots over 800 robot hours. Zeng et al. [30] and Zeng et al. [31] demonstrated on-robot learning by encoding the Q function using a fully convolutional network, but only in the context of open-loop tasks where the gripper performed a pre-defined behavior. FERM [32] performed on-robot learning using SAC [9] in combination with a contrastive learning objective [17, 14], but only for tasks where the orientation of the gripper was fixed. Relative to the work above, our method is most comparable to FERM [32], and we therefore benchmark our method against that.

III. PRELIMINARIES

A. Rotation Group and Representation

The group $\text{SO}(2)$ contains all continuous planar rotations: $\text{SO}(2) = \{\text{Rot}_\theta : 0 \leq \theta < 2\pi\}$. The cyclic group C_n is the discrete subgroup of $\text{SO}(2)$, $C_n = \{\text{Rot}_\theta : \theta \in \{\frac{2\pi i}{n} | 0 \leq i < n\}\}$. $\text{SO}(2)$ (and C_n) has a set of *actions* that formalize how vectors or feature maps transform under rotation. We focus on two types of actions:

1. $\text{SO}(2)$ acts on \mathbb{R} through the *trivial representation* ρ_0 . Let $g \in \text{SO}(2)$ and $x \in \mathbb{R}$. Then $\rho_0(g)x = x$. ρ_0 represents invariance under rotation, for example, how pixel color/depth values change when an image is rotated, i.e. they do not change.
2. $\text{SO}(2)$ acts on \mathbb{R}^2 through the *standard representation* ρ_1 . Let $g \in \text{SO}(2)$ and $v \in \mathbb{R}^2$. Then $\rho_1(g)v = \begin{pmatrix} \cos g & -\sin g \\ \sin g & \cos g \end{pmatrix}v$. This describes how elements of a vector field, e.g., a vector (x, y) transform when rotated.

B. Equivariance

Equivariant and invariant functions can describe symmetries of its input and output with respect to a group G . A function f is G -invariant if when its input x is transformed by a symmetry group element $g \in G$, its output stays the same:

$$f(gx) = f(x). \quad (1)$$

A function f is G -equivariant if when its input x is transformed by a symmetry group element $g \in G$, its output transforms accordingly by g :

$$f(gx) = gf(x). \quad (2)$$

C. G -invariant MDP

A G -invariant MDP [26] is a type of MDP associated with a group G with the following assumptions:

- 1) The reward function $R : S \times A \rightarrow \mathbb{R}$ is G -invariant, that is, for $g \in G$, $R(s, a) = R(gs, ga)$.
- 2) The transition function $T : S \times A \times S \rightarrow \mathbb{R}$ is $\text{SO}(2)$ -invariant, that is, for $g \in G$, $T(s, a, s') = T(gs, ga, s')$.

Wang et al. [26] prove that the optimal Q -function of a G -invariant MDP is G -invariant: $Q^*(s, a) = Q^*(gs, ga)$ and the optimal policy function of a G -invariant MDP is G -equivariant: $\pi^*(gs) = g\pi^*(s)$. This suggests that one can use equivariant functions to encode those two functions to dramatically increase the sample efficiency.

The $\text{SO}(2)$ symmetry of a large number of robotic manipulation tasks can be described as an $\text{SO}(2)$ -invariant MDP ($G = \text{SO}(2)$). For example, in a grasping task where the goal is to pick up an object on the table, the planar rotation of both the state and action will not change the outcome of an action.

D. Equivariant SAC

Based on the properties of $\text{SO}(2)$ -invariant MDP, Equivariant SAC [26] implements an $\text{SO}(2)$ -invariant critic network q and an $\text{SO}(2)$ -equivariant actor network π . Let \mathcal{F}_s be an image representing the state s such that rotating \mathcal{F}_s (i.e., $g\mathcal{F}_s$ where $g \in \text{SO}(2)$) represents the rotation of the state. Let a be the action such that ga represents the rotation of the action. The equivariant property of the actor network π is:

$$\pi(g\mathcal{F}_s) = g\pi(\mathcal{F}_s). \quad (3)$$

The invariant property of the critic network q is:

$$q(g\mathcal{F}_s, ga) = q(\mathcal{F}_s, a). \quad (4)$$

This is illustrated in Figure 1. Assuming the action space is $(x, y, z, \theta, \lambda)$ where λ is the gripper aperture, (x, y, z) is the gripper position displacement, and θ is the gripper orientation displacement along the z -axis. The rotation of the action ga is represented by rotating the (x, y) vector while leaving the other action components unchanged (i.e., $ga = (\rho_1(g)(x, y), z, \theta, \lambda)$). When the state is rotated ($\mathcal{F}_s \rightarrow g\mathcal{F}_s$), the (x, y) vector from the output of the equivariant policy network π is rotated by the same amount ($a \rightarrow ga$). When the state and the action are rotated by the same amount ($(\mathcal{F}_s, a) \rightarrow (g\mathcal{F}_s, ga)$), the output Q -value from the invariant critic network q doesn’t change.

IV. PROBLEM STATEMENT

A. On-Robot Policy Learning

This paper focuses on the *on-robot policy learning* setting which we define as follows.

Definition IV.1 (On-Robot Policy Learning). *In on-robot policy learning, the agent learns a policy from scratch on a physical robot without transfer from any other domain or task. In particular:*

- 1) No pre-training: *The agent does not pretrain any part of its model using an off-line dataset, experience gained from performing a different task, or simulated experiences.*
- 2) No simulation: *The agent does not leverage a simulator during learning.*
- 3) Limited Demonstrations: *The agent has access to a small amount of expert demonstration data from a human or algorithm demonstrator.*

The requirement that all learning must occur on a physical robot is perhaps too extreme – certainly good simulations and large off-line datasets are sometimes available. However, there are many application scenarios where this is not the case and many robotic systems are difficult to model accurately. Moreover, learning on a physical robot forces us to deal with the underlying constraints of sample-based policy learning.

B. On-Robot Learning as an $SO(2)$ -invariant MDP

We formulate our policy learning problem as a Markov Decision Process (MDP) $M = (S, A, T, R, \gamma)$. State $\mathcal{F}_s \in S$ is represented by an n-channel image. Action is a tuple, $a = (x, y, z, \theta, \lambda) \in A \subset \mathbb{R}^5$, where (x, y, z) denotes the positional displacement of the gripper, θ denotes the rotational displacement of the gripper along the z axis, and λ denotes the aperture of the gripper. State and action are assumed to be defined in the same reference frame with the image that encodes state orthogonal to the z -direction in the action space. We define the $SO(2)$ group action on the state by rotating the state image $g\mathcal{F}_s$. We define the $SO(2)$ group action on the MDP action a by rotating the (x, y) vector and leaving the other component unchanged: $ga = (\rho_1(g)(x, y), z, \theta, \lambda)$. In many situations, the MDP described above has a transition and reward function that is invariant to group operations in $SO(2)$. As such, the MDP is $SO(2)$ -invariant (see Section III-C) and can be solved using Equivariant SAC [26].

V. ALGORITHMIC CHOICES IN EQUIVARIANT SAC

It is essential to optimize the sample efficiency of Equivariant SAC to enable it to learn a policy within a minimal amount of environmental steps. In this section, we explore different algorithmic variations of Equivariant SAC in simulation to optimize its sample efficiency. We focus on three main domains of variation: 1) the symmetry groups with respect to which the equivariant networks are defined, 2) different approaches to combining equivariant learning with data augmentation, and 3) ways of incorporating expert demonstrations.

Equivariant Group	$C_4 / C_8 / D_4 / D_8 / SO(2) / O_2$
Buffer Augmentation	yes / no
Number of Buffer Augmentation	0 / 2 / 4 / 8 / 16
Auxiliary Equivariant Loss	yes / no
RAD [13]	yes / no
Number of Expert Demonstration	0 / 10 / 20 / 40
Auxiliary Imitation Loss	yes / no

TABLE I
THE ALGORITHMIC VARIATIONS OF INTEREST AND THEIR DEFAULT SETTINGS (IN BOLD).

Table I shows the algorithmic variations that we explore in this section and their default (optimized) setting. Specifically, we define the equivariant networks in the Dihedral group D_4 (the full network architecture is shown in Appendix A); we perform $SO(2)$ data augmentation in the replay buffer such that every time a new transition is added to the buffer, four augmented transitions will be created and added to the buffer by randomly rotating the transition; and we include 20 episodes of expert demonstration to the replay buffer before the start of training. In each experiment in this section, we modify one corresponding variation and keep the other variations at the default setting (unless otherwise specified).

A. Simulation Environments

We conduct our experiments in four different simulation environments that require different manipulation skills. All tasks have sparse rewards, i.e., +1 reward for reaching the goal, and 0 otherwise. See the detailed description of the environments in Appendix B

Block Picking: The robot needs to grasp a block (Figure 2a). The initial pose of the block is randomly sampled. This is the easiest task.

Clutter Grasping: The robot needs to grasp an object from a clutter of at most five objects (Figure 2b). Both the shapes of the objects and the initial pose of the objects are random.

Block Pushing: The robot needs to push a block to a goal area (Figure 2c). Both the initial pose of the block and the position of the goal are random.

Block in Bowl: The robot needs to pick up a block and place it inside a bowl (Figure 2d). Both the initial pose of the block and the initial position of the bowl are random.

We use a 2-channel image as the observation. The first channel is a top-down depth image centered with respect to the robot gripper. The gripper is drawn at the center of the depth image with its current aperture and orientation. The second channel is a binary channel (i.e., the values of all pixels are either 0 or 1), indicating if the gripper is holding an object. The action space is: $x, y, z \in [-0.05m, 0.05m]; \theta \in [-\frac{\pi}{4}, \frac{\pi}{4}]; \lambda \in [0, 1]$ (0 means fully close and 1 means fully open). Appendix F shows an experiment comparing the selected action space with other candidate action spaces.

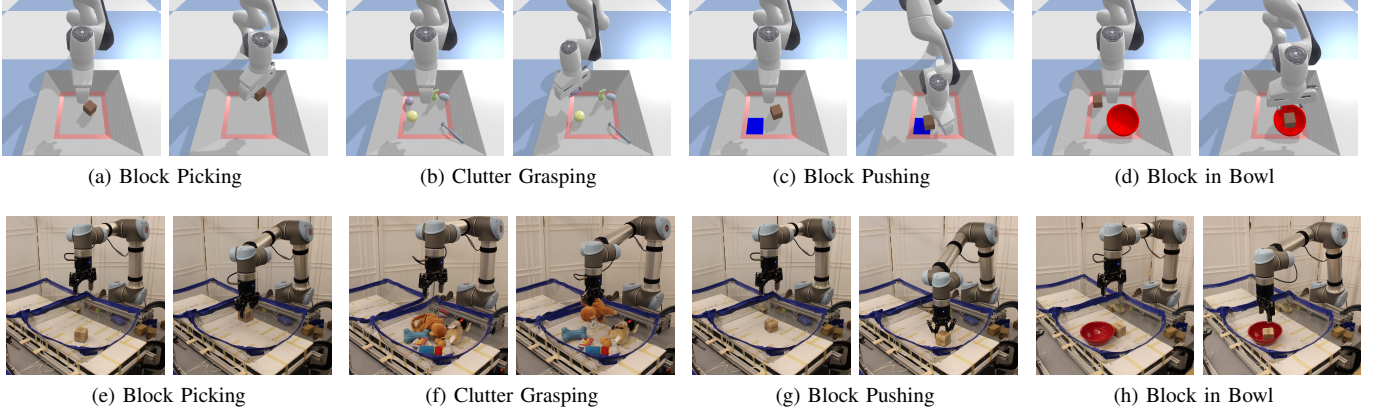


Fig. 2. (a)-(d): Our simulation environments implemented in PyBullet [5]. The left images in each environment show the initial state of the environment; the right images in each environment show the goal state. (e)-(h): Our on-robot learning environments.

B. Equivariant Group

Equation 3 and Equation 4 describes the equivariant and invariant properties of the actor and critic network with respect to the group $SO(2)$. However, when implementing $SO(2)$ -equivariant functions using equivariant networks, it is common in the literature to define the network using the discrete subgroup C_n of $SO(2)$ [4, 28]. Moreover, we find that the properties defined in Equation 3 and Equation 4 also apply to reflection, i.e., one can define the network in the group $O(2)$ or its discrete subgroup D_n (the Dihedral group) to incorporate reflectional symmetry into the network, resulting in an $O(2)$ -Equivariant SAC.

The choice of the group in an equivariant network is essential because it directly describes the symmetry that the network encodes. Moreover, as is shown by Weiler and Cesa [28], a larger group does not necessarily improve the performance of the network. In this experiment, we evaluate the performance of the Equivariant SAC defined in different groups.

1) *Discrete Group*: We first evaluate Equivariant SAC defined in different discrete groups, C_n and D_n . We consider four different variations: 1) C_4 , the cyclic group that encodes four rotations every 90 degrees; 2) C_8 , the cyclic group that encodes eight rotations every 45 degrees; 3) D_4 , the Dihedral group that encodes four rotations every 90 degrees and reflection; 4) D_8 , the Dihedral group that encodes eight rotations every 45 degrees and reflection. Figure 3 shows the result. In all four environments, D_4 shows the best performance over the four different groups. Note that even though D_8 encodes more rotations than D_4 , its performance does not surpass D_4 .

2) *Continuous Group*: This experiment evaluates Equivariant SAC defined for the continuous group $SO(2)$ or $O(2)$ with a baseline of D_4 . As is shown in Figure 4, Equivariant SAC defined over $O(2)$ (green) has a marginal improvement over that defined over $SO(2)$ (red). The improvement of incorporating reflectional symmetry mirrors our finding in Section V-B1 where the Dihedral group outperforms the cyclic group. However, both the $SO(2)$ and $O(2)$ networks underperform the D_4 network (blue). This is because the

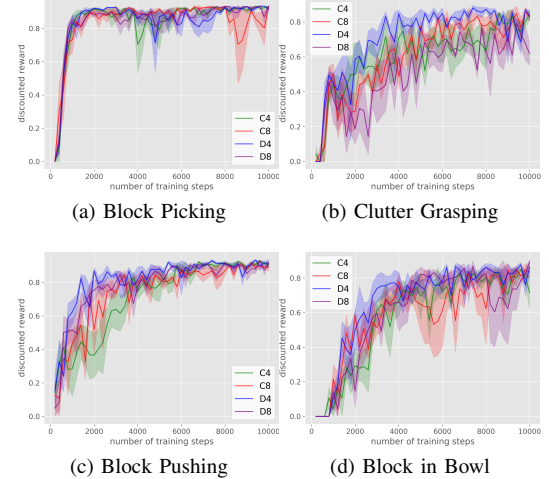
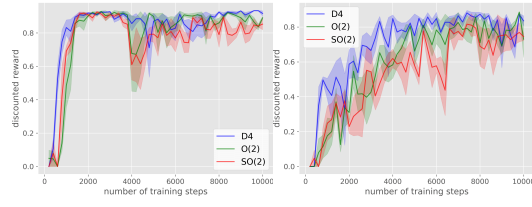


Fig. 3. Comparison of Equivariant SAC defined in different discrete groups. The plots show the performance of the behavior policy in terms of the discounted reward. Each point is the average discounted reward in the previous 200 steps. Results are averaged over four runs. Shading denotes standard error.

D_4 network has access to the *regular representation* as the hidden layer of the network. In contrast, the networks defined in the continuous group do not (since only finite groups have the regular representation). The regular representation explicitly encodes the feature over all elements in the finite group, making it an informative representation for the hidden layers. Moreover, the regular representation is compatible with component-wise activation functions and component-wise max pooling, which are most commonly used and known to work well in deep networks. Such a performance distinction between the discrete group and the continuous group is also illustrated in [28].

C. Combining Data Augmentation With Equivariant Learning

Section V-B suggests that the best performing networks are not constrained to be equivariant to the full group of symmetries $O(2)$, but only to a subset of the them $D_4 \subset O(2)$. Since D_4 only enforces equivariance to rotations which are a



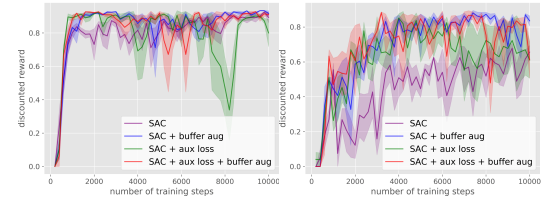
(a) Block Picking

(b) Clutter Grasping

(c) Block Pushing

(d) Block in Bowl

Fig. 4. Comparison of Equivariant SAC defined in D_4 and $SO(2)$. The plots show the performance of the behavior policy in terms of the discounted reward. Each point is the average discounted reward in the previous 200 steps. Results are averaged over four runs. Shading denotes standard error.



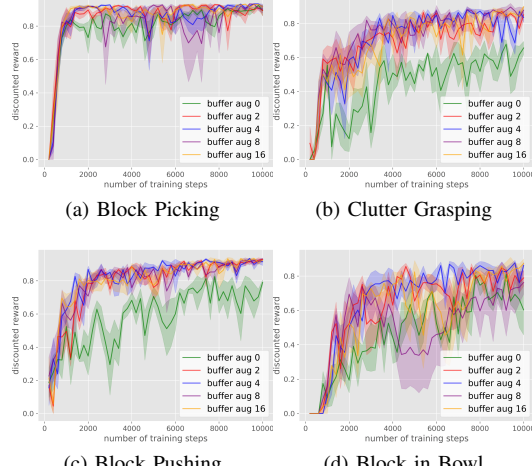
(a) Block Picking

(b) Clutter Grasping

(c) Block Pushing

(d) Block in Bowl

Fig. 6. Comparison of Equivariant SAC equipped with an auxiliary equivariant loss. The plots show the performance of the behavior policy in terms of the discounted reward. Each point is the average discounted reward in the previous 200 steps. Results are averaged over four runs. Shading denotes standard error.



(a) Block Picking

(b) Clutter Grasping

(c) Block Pushing

(d) Block in Bowl

Fig. 5. Comparison of Equivariant SAC equipped with rotational data augmentation in the replay buffer. The plots show the performance of the behavior policy in terms of the discounted reward. Each point is the average discounted reward in the previous 200 steps. Results are averaged over four runs. Shading denotes standard error.

multiple of $\pi/2$, the agent still needs to actively learn the rotational symmetry within a continuous range $(0, \frac{\pi}{2})$ in order to be fully $O(2)$ -equivariant.

In this experiment, we explore the use of data augmentation techniques in combination with equivariant learning to better encode the desired equivariant functions. We consider three different rotational data augmentation methods: 1) conducting data augmentation in the replay buffer through creating extra transitions using $SO(2)$ rotations; 2) applying an auxiliary equivariant loss to enforce equivariance; 3) using RAD [13] to perform data augmentation at each sample and training step.

1) *Buffer Augmentation*: The most trivial data augmentation method is creating additional samples using random

$SO(2)$ rotations and adding them to the buffer. We consider five different numbers of augmentations for each transition: 0, 2, 4, 8, and 16 (0 means no extra augmented transition is added). Figure 5 shows the result. First, note that no augmentation at all (green) is always the worst-performing variation, suggesting that providing extra augmented samples to the agent is beneficial. Second, note that more augmentation does not necessarily mean better performance (e.g., buffer aug 8 (purple) and buffer aug 16 (orange) underperforms buffer aug 4 (blue) in Block in Bowl). Four augmentations (blue) shows the best performance overall.

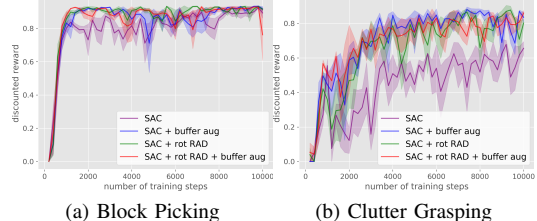
2) *Auxiliary Equivariant Loss*: The second data augmentation technique we consider is using an auxiliary equivariant loss:

$$\mathcal{L}_{\text{aux}}^{\text{actor}} = \frac{1}{2}(\pi(g\mathcal{F}_s) - g\pi(\mathcal{F}_s))^2, \quad (5)$$

$$\mathcal{L}_{\text{aux}}^{\text{critic}} = \frac{1}{2}(q(g\mathcal{F}_s, ga) - q(\mathcal{F}_s, a))^2, \quad (6)$$

where $g \in SO(2)$, (\mathcal{F}_s, a) is the sampled state-action pair in the minibatch. The auxiliary losses are added to the original SAC loss to enforce the equivariant and invariant properties in Equation 3 and 4. In this experiment, we consider four variations: 1) SAC: vanilla Equivariant SAC with no data augmentation at all; 2) SAC + buffer aug: Equivariant SAC with four $SO(2)$ data augmentations in the buffer; 3): SAC + aux loss: Equivariant SAC with auxiliary equivariant loss; 4): SAC + aux loss + buffer aug: Equivariant SAC with both the auxiliary equivariant loss and four $SO(2)$ data augmentations in the buffer.

Figure 6 shows the result. First, note that the auxiliary equivariant loss (green) performs equally well as performing data augmentation in the buffer (blue) in two (Block Pushing and Block in Bowl) of the four environments. In the other two environments the auxiliary loss is less stable. Second,



(a) Block Picking

(b) Clutter Grasping

(c) Block Pushing

(d) Block in Bowl

Fig. 7. Comparison of Equivariant SAC equipped with rotational data augmentation using RAD. The plots show the performance of the behavior policy in terms of the discounted reward. Each point is the average discounted reward in the previous 200 steps. Results are averaged over four runs. Shading denotes standard error.

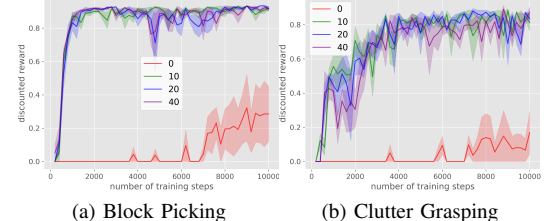
combining the auxiliary loss with buffer augmentation (red) does not improve more than performing a single augmentation.

3) *Rot RAD*: The third data augmentation approach that we evaluate is RAD [13]. The original version of RAD performs a data augmentation step using a random crop operator after sampling a minibatch from the buffer. We modify the data augmentation operator from random crop to random SO(2) rotation to enforce the network to learn the desired equivariant property. An experiment using the original random crop data augmentation is shown in Appendix G. We consider four variations: 1) SAC: Equivariant SAC with no data augmentation; 2): SAC + buffer aug: Equivariant SAC with four SO(2) data augmentation in the buffer; 3): SAC + rot RAD: Equivariant SAC with RAD implemented with a SO(2) rotation operator; 4): SAC + rot RAD + buffer aug: 3) with additional four SO(2) data augmentation in the buffer. Figure 7 shows the result. Note that the versions of Equivariant SAC equipped with SO(2) RAD (green and red) perform nearly as well as Equivariant SAC with buffer augmentation (blue).

Combining the results of this section and those in Section V-C1 and Section V-C2, we can conclude that even though Equivariant SAC already encodes D4 equivariance within the structure of the network, adding SO(2) data augmentations to the algorithm can still benefit it by a substantial margin, especially in the challenging tasks. However, the three different data augmentation techniques that we explore in these sections do not show a significant difference compared with each other. Buffer augmentation is the simplest and most stable solution.

D. Effect of Expert Demonstration

Expert demonstrations are critical when solving challenging sparse rewards tasks. Without it, the agent must search randomly for a goal state and this can take a long time. This section evaluates two essential factors in injecting expert



(a) Block Picking

(b) Clutter Grasping

(c) Block Pushing

(d) Block in Bowl

Fig. 8. Comparison of Equivariant SAC with different amount of expert demonstration episodes. The plots show the performance of the behavior policy in terms of the discounted reward. Each point is the average discounted reward in the previous 200 steps. Results are averaged over four runs. Shading denotes standard error.

demonstration to Equivariant SAC: the number of expert demonstrations needed and if a behavior cloning loss will be beneficial.

1) *Number of Expert Demonstration*: This experiment studies two questions: 1) if expert demonstration is necessary when using Equivariant SAC to solve our tasks; 2) if it is necessary, how many demonstrations are needed. We consider four different amount of expert demonstration episodes provided to the agent: 0, 10, 20, and 40. Figure 8 shows the comparison result. First, note that expert demonstration is always required since the variation without any demonstration (red) struggles to learn a good policy in all four environments. Second, we found that the Equivariant SAC can do well with just 10 or 20 expert demonstrations. The fact that we require so few demonstrations is especially important in situations where it is a human who must provide the demonstrations.

2) *SACfD*: In this experiment, we evaluate if an auxiliary demonstration loss will be beneficial for Equivariant SAC. We use SACfD [26] as the baseline for incorporating a demonstration loss to the actor:

$$\mathcal{L}_{\text{SACfD}}^{\text{actor}} = \mathbb{1}_e \left[\frac{1}{2} ((a \sim \pi(s)) - a_e)^2 \right], \quad (7)$$

where $\mathbb{1}_e = 1$ if the sampled transition is an expert demonstration and 0 otherwise, $a \sim \pi(s)$ is an action sampled from the output Gaussian distribution of $\pi(s)$, and a_e is the expert action. This demonstration loss is used in addition to the loss of SAC to incline its policy to the expert policy. Figure 9 shows the comparison between Equivariant SACfD (green) and Equivariant SAC (blue). Interestingly, Equivariant SACfD outperforms Equivariant SAC in three of the environments, but underperforms in Clutter Grasping. This is because the expert policy for Clutter Grasping is sub-optimal (since the planner does not have access to the optimal grasping point of each random object), while the expert for the other three tasks

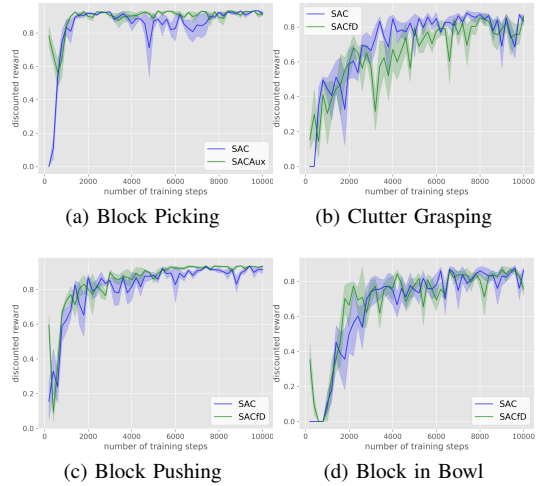


Fig. 9. Comparison of Equivariant SAC with Equivariant SAC from Demonstration (SACfD). The plots show the performance of the behavior policy in terms of the discounted reward. Each point is the average discounted reward in the previous 200 steps. Results are averaged over four runs. Shading denotes standard error.

are nearly optimal. The performance of SACfD indicates that when the expert demonstration is sub-optimal, an auxiliary demonstration loss will harm the performance of Equivariant SAC. This is an important finding because the planner that generates the expert policy in on-robot learning is often sub-optimal (since it does not have access to the pose of the objects as in the simulation).

E. Summary of Findings

We sum up the findings of this section as follows:

- 1) The Equivariant SAC defined over the group D_4 has the best performance.
- 2) Using data augmentation techniques with the equivariant network is important, but different data augmentation approaches show similar performance.
- 3) A small amount of expert demonstration is essential for Equivariant SAC, but an auxiliary demonstration loss can be harmful when the demonstration policy is sub-optimal.

Per our findings from the simulation experiments, we use the algorithmic settings as shown in Table I in our on-robot learning experiment.

VI. ON-ROBOT LEARNING EXPERIMENT

A. Experimental Setup

This section evaluates the optimized Equivariant SAC in on-robot learning. Our experimental setup is shown in Figure 10. The experiment is conducted on a Universal Robots UR5 arm equipped with a Robotiq 2F-85 parallel-jaw gripper. We use one Occipital Structure Sensor and one Microsoft Azure Kinect DK mounted above the robot to generate the observation. Our workstation has a Intel Core i7-9700k CPU (3.60GHz) and a Nvidia RTX 2080Ti GPU. During training, each training step takes approximately 1.1 seconds, including

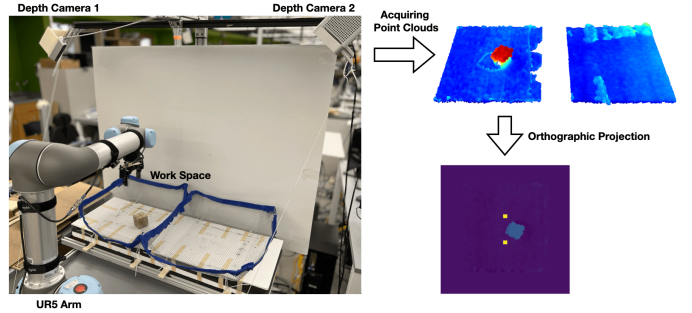


Fig. 10. Our experimental set up for on-robot learning. The observation (bottom right) is generated by first acquiring point clouds from two depth cameras above the workspace then creating an orthographic projection at the gripper's position. The gripper is drawn at the center of the observation (in yellow) with its current aperture and orientation.

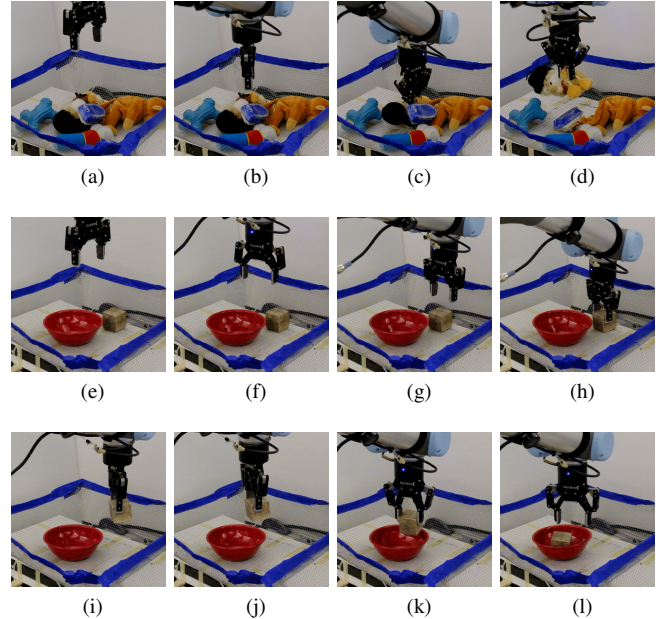


Fig. 11. (a)-(d): One example episode of Clutter Grasping. (e)-(l): One example episode of Block in Bowl.

one SGD step and one environmental step running in parallel. Two bins in front of the robot make up the workspace. We experiment with the same four tasks (Block Picking, Clutter Grasping, Block Pushing, Block in Bowl) as in Section V. Figure 2 (e)-(f) shows those environments on the physical robot. Note that in Block Pushing, we use a virtual goal drawn on the observation, so the goal is visible to the agent but not to the observer. In tasks that involve a single object (Block Picking and Block Pushing), the robot will only use one bin as the workspace. In tasks involving multiple objects (Clutter Grasping and Block in Bowl), the robot will iteratively use one of the two bins as the active workspace and use the other bin to reset the environment.

We implement an automated resetting process for all four environments. In Block Picking and Block Pushing, the robot will reset the environment through picking up the block

Task	Block Picking	Clutter Grasping	Block Pushing	Block in Bowl
Number of training steps	2000	2000	2000	4000
Approximate time for training	45 minutes	45 minutes	1 hour	2 hours 40 minutes
Evaluation success rate	100% (50/50)	96% (48/50)	92% (46/50)	92% (46/50)

TABLE II

THE NUMBER OF TRAINING STEPS, APPROXIMATE TIME FOR TRAINING, AND THE REVALUATION SUCCESS RATE OF THE TRAINED POLICY OF OUR ON-ROBOT LEARNING.

and randomly placing it inside the workspace. In Block in Bowl, the robot will move both the bowl and the block from the active workspace to random positions in the reset bin, then switch the active workspace to the reset bin. In Clutter Grasping, after the robot successfully grasps one object from the active workspace, it will drop the object to a random position in the reset bin. Once the robot grasps all objects from the active workspace, the robot will switch the active workspace to the reset bin. See Appendix C for more details.

B. Statement of Results

Table II shows the statistics of our on-robot learning. In Block Picking, Clutter Grasping, and Block Pushing, the Equivariant SAC only requires 2000 steps for learning the policy, which is approximately 45 minutes in total, including the time required for resetting the environment (in block pushing, 2000 steps takes one hour because the resetting takes slightly longer than Block Picking and Clutter Grasping). In Block in Bowl, Equivariant SAC takes 4000 steps to converge, which is 2 hours and 40 minutes. This includes around 73 minutes ($1.1s \times 4000$) of environmental steps and 107 minutes for resetting the environment. Figure 11 shows an example episode of Clutter Grasping and one example episode of Block in Bowl.

We evaluate our trained policy for each task for 50 episodes. In Block Picking, the robot succeeds in all trials. In Clutter Grasping, the robot failed to find an appropriate grasp point in two episodes. In Block Pushing, the robot fails to move towards the block in two episodes. In the other two failures, the robot keeps pushing down from the top of the block. In Block in Bowl, the robot grasps the block but does not move towards the bowl in three episodes. In the other failure, the robot grasps the bowl and the block simultaneously and doesn't release them.

C. Comparison with Baseline

We evaluate the Equivariant SAC with the FERM [32] baseline. FERM utilizes contrastive learning with random crop augmentations to improve the sample efficiency in on-robot learning. We implement FERM such that the image encoder has a similar amount of trainable parameters as the equivariant network (1.5M vs 1.1M). Appendix E shows the details of the baseline.

Figure 12 shows the learning curve comparison between Equivariant SAC and the FERM baseline. In Block Picking, Equivariant SAC masters the task after about 1000 steps, while

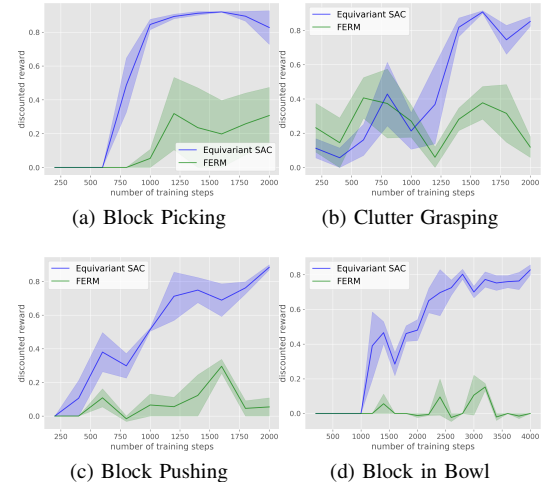


Fig. 12. Comparison of Equivariant SAC with FERM in real world on-robot learning. The plots show the performance of the behavior policy in terms of the discounted reward. Each point is the average discounted reward in the previous 200 steps. Results are averaged over three runs. Shading denotes standard error.

FERM learns slower and converges to a sub-optimal policy. In Clutter Grasping, FERM performs better at the beginning phase of learning but fails to converge to a good policy at the end of learning. We hypothesis that this is because: 1) the pre-training of the encoder in FERM helps the network to learn a better feature representation at the early phase of learning. 2) this task does not require accurate manipulation as the other three tasks since the objects are all deformable (this also explains why the on-robot learning is faster than the simulation in this task). In Block Pushing and Block in Bowl, FERM fails to learn any good policy at all, while Equivariant SAC solves the task within 2000 and 4000 steps, respectively.

VII. DISCUSSION

This paper demonstrates on-robot learning using Equivariant SAC [26]. We evaluate several algorithmic choices in Equivariant SAC on performance and conclude the following: 1) the symmetry group $D4 \subset O(2)$ performs best; 2) data augmentation is important, but the type of data augmentation does not make much of a difference; 3) a small number of expert demonstrations are necessary, but no more than 20 demonstrations are needed per task. Ultimately, we demonstrate that $O(2)$ -Equivariant SAC with the algorithmic choices summarized in Table I can be used to learn policies that can

solve various challenging robotic manipulation tasks in an hour or two (Table II).

This work has several limitations and directions for future works. First, to satisfy the assumptions of a G -invariant MDP, we need to remove the robot arm and gripper from the point cloud before generating the orthographic projection. This becomes problematic when the gripper is making contact with the objects since either part of the object will be removed from the point cloud, or the gripper will remain in the point cloud. Pursuing an equivariant architecture that is robust in the presence of the robot arm will be an essential direction of future work. Second, since we are training on the robot without human supervision, we must: 1) be able to automatically check for task completion; 2) be able to reset the environment at the end of a task. Both of these things are potentially challenging to implement. Finally, given the challenges of RL on physical robotic systems, another avenue for future work would be to develop equivariant methods that can learn entirely from human demonstration.

REFERENCES

- [1] Gregory Benton, Marc Finzi, Pavel Izmailov, and Andrew Gordon Wilson. Learning invariances in neural networks. *arXiv preprint arXiv:2010.11882*, 2020.
- [2] Ondrej Biza, Dian Wang, Robert Platt, Jan-Willem van de Meent, and Lawson LS Wong. Action priors for large action spaces in robotics. *arXiv preprint arXiv:2101.04178*, 2021.
- [3] Taco Cohen and Max Welling. Group equivariant convolutional networks. In *International conference on machine learning*, pages 2990–2999. PMLR, 2016.
- [4] Taco S Cohen and Max Welling. Steerable cnns. *arXiv preprint arXiv:1612.08498*, 2016.
- [5] Erwin Coumans and Yunfei Bai. Pybullet, a python module for physics simulation for games, robotics and machine learning. *GitHub repository*, 2016.
- [6] Neel Dey, Antong Chen, and Soheil Ghafurian. Group equivariant generative adversarial networks. *arXiv preprint arXiv:2005.01683*, 2020.
- [7] Shixiang Gu, Ethan Holly, Timothy Lillicrap, and Sergey Levine. Deep reinforcement learning for robotic manipulation with asynchronous off-policy updates. In *2017 IEEE international conference on robotics and automation (ICRA)*, pages 3389–3396. IEEE, 2017.
- [8] Marcus Gualtieri and Robert Platt. Learning manipulation skills via hierarchical spatial attention. *IEEE Transactions on Robotics*, 36(4):1067–1078, 2020.
- [9] Tuomas Haarnoja, Aurick Zhou, Pieter Abbeel, and Sergey Levine. Soft actor-critic: Off-policy maximum entropy deep reinforcement learning with a stochastic actor. In *International conference on machine learning*, pages 1861–1870. PMLR, 2018.
- [10] Dmitry Kalashnikov, Alex Irpan, Peter Pastor, Julian Ibarz, Alexander Herzog, Eric Jang, Deirdre Quillen, Ethan Holly, Mrinal Kalakrishnan, Vincent Vanhoucke, et al. Qt-opt: Scalable deep reinforcement learning for vision-based robotic manipulation. *arXiv preprint arXiv:1806.10293*, 2018.
- [11] Diederik P Kingma and Jimmy Ba. Adam: A method for stochastic optimization. *arXiv preprint arXiv:1412.6980*, 2014.
- [12] Ilya Kostrikov, Denis Yarats, and Rob Fergus. Image augmentation is all you need: Regularizing deep reinforcement learning from pixels. *arXiv preprint arXiv:2004.13649*, 2020.
- [13] Michael Laskin, Kimin Lee, Adam Stooke, Lerrel Pinto, Pieter Abbeel, and Aravind Srinivas. Reinforcement learning with augmented data. *arXiv preprint arXiv:2004.14990*, 2020.
- [14] Michael Laskin, Aravind Srinivas, and Pieter Abbeel. Curl: Contrastive unsupervised representations for reinforcement learning. In *International Conference on Machine Learning*, pages 5639–5650. PMLR, 2020.
- [15] Sergey Levine, Peter Pastor, Alex Krizhevsky, Julian Ibarz, and Deirdre Quillen. Learning hand-eye coordination for robotic grasping with deep learning and large-scale data collection. *The International Journal of Robotics Research*, 37(4-5):421–436, 2018.
- [16] Arnab Kumar Mondal, Pratheeeksha Nair, and Kaleem Siddiqi. Group equivariant deep reinforcement learning. *arXiv preprint arXiv:2007.03437*, 2020.
- [17] Aaron van den Oord, Yazhe Li, and Oriol Vinyals. Representation learning with contrastive predictive coding. *arXiv preprint arXiv:1807.03748*, 2018.
- [18] Adam Paszke, Sam Gross, Soumith Chintala, Gregory Chanan, Edward Yang, Zachary DeVito, Zeming Lin, Alban Desmaison, Luca Antiga, and Adam Lerer. Automatic differentiation in PyTorch. In *NIPS Autodiff Workshop*, 2017.
- [19] Lerrel Pinto and Abhinav Gupta. Supersizing self-supervision: Learning to grasp from 50k tries and 700 robot hours. In *2016 IEEE international conference on robotics and automation (ICRA)*, pages 3406–3413. IEEE, 2016.
- [20] Andrei A Rusu, Matej Večerík, Thomas Rothörl, Nicolas Heess, Razvan Pascanu, and Raia Hadsell. Sim-to-real robot learning from pixels with progressive nets. In *Conference on Robot Learning*, pages 262–270. PMLR, 2017.
- [21] Avi Singh, Larry Yang, Kristian Hartikainen, Chelsea Finn, and Sergey Levine. End-to-end robotic reinforcement learning without reward engineering. *arXiv preprint arXiv:1904.07854*, 2019.
- [22] Elise van der Pol, Daniel Worrall, Herke van Hoof, Frans Oliehoek, and Max Welling. Mdp homomorphic networks: Group symmetries in reinforcement learning. *Advances in Neural Information Processing Systems*, 33, 2020.
- [23] Robin Walters, Jinxi Li, and Rose Yu. Trajectory prediction using equivariant continuous convolution. *arXiv preprint arXiv:2010.11344*, 2020.
- [24] Dian Wang, Colin Kohler, and Robert Platt. Pol-

icy learning in se (3) action spaces. *arXiv preprint arXiv:2010.02798*, 2020.

- [25] Dian Wang, Robin Walters, Xupeng Zhu, and Robert Platt. Equivariant q learning in spatial action spaces. In *5th Annual Conference on Robot Learning*, 2021. URL <https://openreview.net/forum?id=IScz42A3iCI>.
- [26] Dian Wang, Robin Walters, and Robert Platt. SO(2)-equivariant reinforcement learning. In *International Conference on Learning Representations*, 2022. URL https://openreview.net/forum?id=7F9cOhdvfk_.
- [27] Rui Wang, Robin Walters, and Rose Yu. Incorporating symmetry into deep dynamics models for improved generalization. *arXiv preprint arXiv:2002.03061*, 2020.
- [28] Maurice Weiler and Gabriele Cesa. General $e(2)$ -equivariant steerable cnns. *arXiv preprint arXiv:1911.08251*, 2019.
- [29] Walter Wohlkinger, Aitor Aldoma, Radu B Rusu, and Markus Vincze. 3dnet: Large-scale object class recognition from cad models. In *2012 IEEE international conference on robotics and automation*, pages 5384–5391. IEEE, 2012.
- [30] Andy Zeng, Shuran Song, Stefan Welker, Johnny Lee, Alberto Rodriguez, and Thomas Funkhouser. Learning synergies between pushing and grasping with self-supervised deep reinforcement learning. In *2018 IEEE/RSJ International Conference on Intelligent Robots and Systems (IROS)*, pages 4238–4245. IEEE, 2018.
- [31] Andy Zeng, Shuran Song, Johnny Lee, Alberto Rodriguez, and Thomas Funkhouser. Tossingbot: Learning to throw arbitrary objects with residual physics. *IEEE Transactions on Robotics*, 36(4):1307–1319, 2020.
- [32] Albert Zhan, Philip Zhao, Lerrel Pinto, Pieter Abbeel, and Michael Laskin. A framework for efficient robotic manipulation. *arXiv preprint arXiv:2012.07975*, 2020.
- [33] Yuke Zhu, Ziyu Wang, Josh Merel, Andrei Rusu, Tom Erez, Serkan Cabi, Saran Tunyasuvunakool, János Kramár, Raia Hadsell, Nando de Freitas, et al. Reinforcement and imitation learning for diverse visuomotor skills. *arXiv preprint arXiv:1802.09564*, 2018.

APPENDIX

A. Network Architecture

Our equivariant neural networks are implemented using the E2CNN [28] library in PyTorch [18]. The network architecture of the discrete group variations (C_4, C_8, D_4, D_8) is illustrated in Figure 19. The actor network π (Figure 19 top) takes in \mathcal{F}_s as a trivial representation feature map. The hidden layers are all implemented using the regular representation. The output of π is a mixed representation feature map with 1×1 spatial dimension (so that it can also be viewed as a vector). This vector consists of $1 \rho_1$ feature, representing the means of the action component (x, y) , and 8 trivial representation features, representing the means of the action component (z, θ, λ) as well as the standard deviations of all action dimensions. The critic network q (Figure 19 bottom) takes in \mathcal{F}_s as a trivial representation feature map. The upper path of q generates a 64 -channel regular representation feature map with 1×1 spatial dimensions. This regular representation feature map is concatenated with the action a , which is encoded as $1 \rho_1$ feature (representing (x, y)) and $3 \rho_0$ features (representing (z, θ, λ)). The concatenated feature map is sent to two separate blocks to generate two Q estimates in the form of 1×1 trivial representation feature map. In both the actor and critic network, we use ReLU as the activation function.

For the continuous group variations ($\text{SO}(2), \text{O}_2$), we define the networks with a maximum frequency of 3 (since the continuous group $\text{SO}(2), \text{O}_2$ have infinite number of irreducible representations, the maximum frequency specifies the maximum frequency of the irreducible representations to build [28]). The forms of the input and output feature types are the same as the discrete group variations. However, for the hidden layers, we use $\rho_0^k \oplus \rho_1^k \oplus \rho_2^k \oplus \rho_3^k$ as the representation type for the $\text{SO}(2)$ network. In principle, $\rho_m(g) = \rho_1(mg)$ describes the rotation symmetries in different frequencies. We use $\rho_0^k \oplus \rho_{(1,0)}^k \oplus \rho_{(1,1)}^k \oplus \rho_{(1,2)}^k \oplus \rho_{(1,3)}^k$ for the hidden layers in the $\text{O}(2)$ network. The group $\text{O}(2)$ is generated by rotations $\text{Rot}(\theta)$ and a reflection f over the x -axis. For $k > 0$, $\rho_{(1,k)}$ is the irreducible representation of $\text{O}(2)$ on \mathbb{R}^2 in which rotations $\text{Rot}(\theta)$ rotate vectors about the origin by $k\theta$ and f reflects vectors over the x -axis. We use the gated nonlinearity as the activation function.

B. Simulation Environment Details

In all simulation environments, the workspace has a size of $0.3m \times 0.3m \times 0.24m$. All workspace is inside a bin with a bounding box size of $0.45m \times 0.45m \times 0.1m$. The bottom size of the bin is $0.3m \times 0.3m$. We use a simulated Franka Panda arm in all simulations. All environments raise a sparse reward, i.e., $+1$ when the agent finishes the task, and 0 otherwise. The maximum time steps for all tasks is 50 . At the beginning of each episode, the gripper is moved to the center of the workspace.

1) *Block Picking*: In the Block Picking environment, the robot needs to pick up a block with a size of $5cm \times 5cm \times 5cm$. At the start of each episode, the block is initialized with

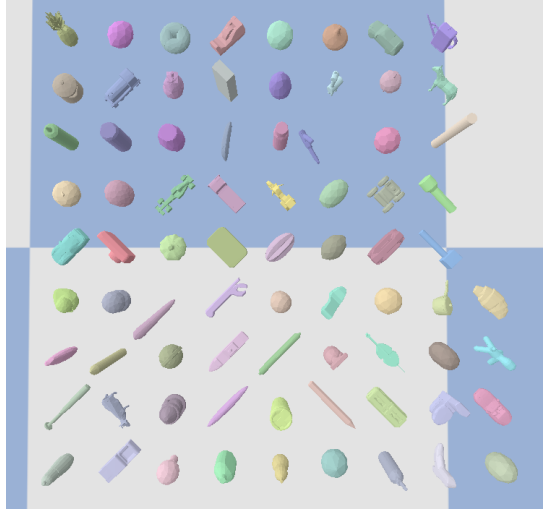


Fig. 13. The object set for Clutter Grasping in simulation contains 76 objects from the 3DNet [29] dataset.

random position and orientation. The goal is to grasp the block and lift it s.t. the gripper is at least $0.15m$ above the ground. The observation in this environment covers an area of $0.3m \times 0.3m$.

2) *Clutter Grasping*: In the Clutter Grasping environment, the robot needs to pick up an object from a clutter of at most five objects. At the start of training, five random objects are initialized with random position and orientation. The shapes of the objects are randomly sampled from the object set shown in Figure 13. The object set contains 76 objects derived from the 3DNet [29] dataset. Every time the agent successfully grasps all five objects, the environment will re-generate five random objects with random positions and orientations. If an episode terminates with any remaining objects in the bin, the object will not be re-initialized. The goal of this task is to grasp any object and lift it s.t. the gripper is at least $0.15m$ above the ground. The observation in this environment covers an area of $0.3m \times 0.3m$.

3) *Block Pushing*: In the Block Pushing environment, the robot needs to push a block with a size of $5cm \times 5cm \times 5cm$ to the goal area with a size of $9cm \times 9cm$. At the start of each episode, the block is initialized with a random position and orientation, and the goal is initialized with a random position at least $9cm$ away from the block. The goal is to push the block s.t. the distance between the block's center and the goal's center is within $5cm$. The observation in this environment covers an area of $0.45m \times 0.45m$. The goal area is drawn on the observation by adding $2cm$ to the height values.

4) *Block in Bowl*: In the Block in Bowl environment, the robot needs to pick up a block with a size of $5cm \times 5cm \times 5cm$ and place it inside a bowl with a bounding box size of $16cm \times 16cm \times 7cm$. At the start of each episode, the block and the bowl are initialized with a random position and orientation. The observation in this environment covers an area of $0.45m \times 0.45m$.



Fig. 14. The object set for on-robot Clutter Grasping

C. On-Robot Learning Details

In the on-robot learning environment, the two bins have a bottom size of $0.25m \times 0.25m$. The bounding box of each bin has a size of $0.4m \times 0.4m \times 0.11m$. The workspace of the arm is inside one of the two bins, with a size of $0.23m \times 0.23m \times 0.2m$. Similar to simulation environments, all real-world environments raise a sparse reward, +1 when success and 0 otherwise. We implement a collision protection algorithm to prevent the arm from colliding with the environment by reading the force applied to the end-effector. A -0.1 reward is given when a protective stop is triggered on the UR5. The maximum number of time steps per episode for all environments is 50. Reset and reward functions are implemented specifically for different tasks as follows.

1) *Block picking*: In the block picking environment, only one bin will be used throughout the training. The block has a size of $5cm \times 5cm \times 5cm$. A reward will be given when the block is grasped and lifted for 0.1m above the ground by reading the signals from the gripper. At the start of each episode, the block is reset to a random position and orientation in the current bin. The observation covers an area of $0.3m \times 0.3m$.

2) *Clutter Grasping*: The Clutter Grasping environment contains a clutter of five objects, as is shown in Figure 14. In this experiment, one bin is used as the active workspace, and the other bin is used as the reset bin. The goal is to grasp an object and lift it to 0.1m above the ground. Once grasped, the object will be reset with random positions and orientations into the reset bin. After all objects in the active workspace are grasped, the active workspace and the reset bin are swapped. This process is shown in Figure 15. If the robot fails to grasp any object for five consecutive episodes, all remaining objects in the active workspace will be moved to the reset bin. The observation covers an area of $0.3m \times 0.3m$.

3) *Block Pushing*: In the Block Pushing environment, only one bin will be used throughout the training. The goal is to move the block s.t. more than 77 pixels of the block are within the goal area. The block has a size of $5cm \times 5cm \times 5cm$. At

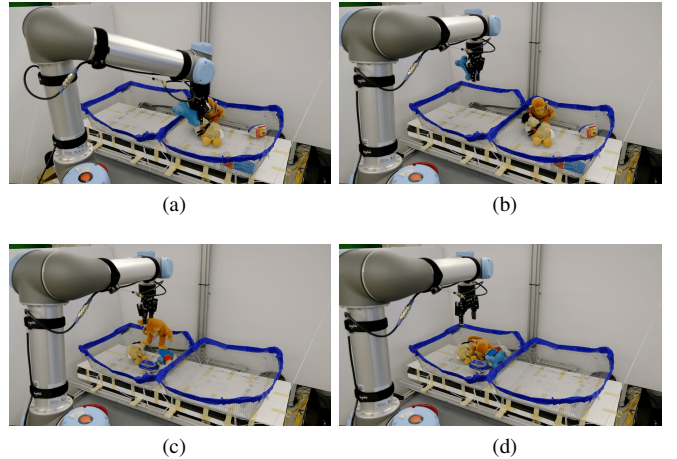


Fig. 15. The reset process of Clutter Grasping. (a) The robot successfully grasps an object in the active workspace (right bin). (b) The robot places the grasped object in the reset bin (left bin). (c) The robot grasps and places the last object from the active workspace (right bin) to the reset bin (left bin). (d) The robot switches the active workspace to the left bin.

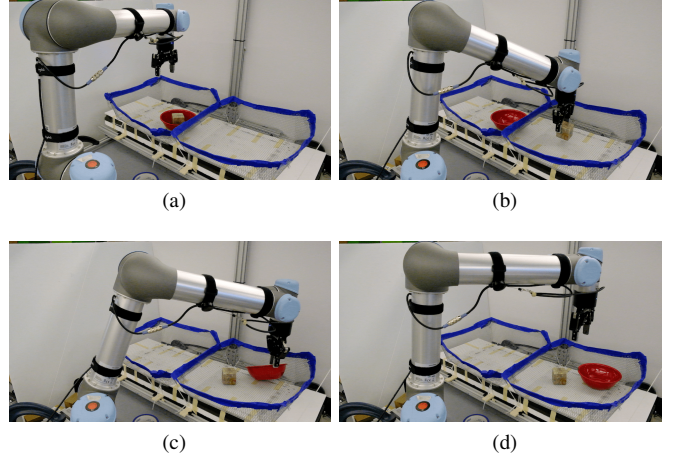
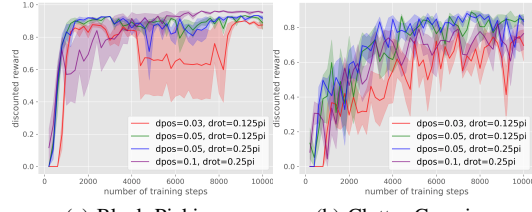


Fig. 16. The reset process of Block in Bowl. (a) The robot finishes an episode in the active workspace (left bin). (b) The robot picks up the block and places it in the reset bin (right bin). (c) The robot picks up the bowl and places it in the reset bin (right bin). (d) The robot switches the active workspace to the right bin.

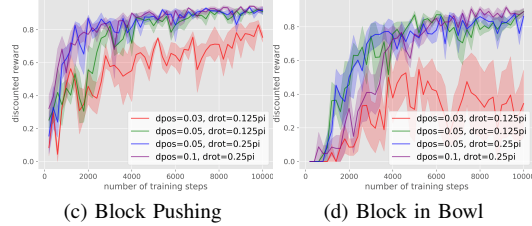
the beginning of each episode, a goal area of $0.77m \times 0.77m$ is virtually generated at least $9cm$ away from the block. The goal area is drawn to the observation by adding the height value by $0.02m$. When resetting, the arm will move the block to a new random position. The observation covers an area of $0.45m \times 0.45m$, in order to get a larger field of view that includes both object and goal area.

4) *Block in Bowl*: In the Block in Bowl environment, we use one bin as the active workspace and the other bin as the reset bin. The goal is to grasp the block and then put it into the bowl. The bowl has a radius of $8cm$ and the block has a size of $5cm \times 5cm \times 5cm$. At the beginning of each episode, both the block and the bowl will be reset into the reset bin with random positions and orientations, keeping at least $14cm$



(a) Block Picking

(b) Clutter Grasping



(c) Block Pushing

(d) Block in Bowl

Fig. 17. Comparison of Equivariant SAC with different action spaces. The plots show the performance of the behavior policy in terms of the discounted reward. Each point is the average discounted reward in the previous 200 steps. Results are averaged over four runs. Shading denotes standard error.

away from each other. The active workspace and the reset bin are then swapped. This process is shown in Figure 16. The reset function utilizes circle detection for grasping the bowl. The observation covers an area of $0.45m \times 0.45m$ to provide a larger view to cover both the block and the bowl.

D. Training Details

The pixel size of the observation is 128×128 for all methods except for the FERM baseline and RAD crop baseline, where the observation’s pixel size is 142×142 and will be cropped to 128×128 .

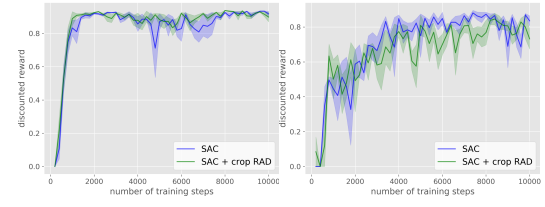
We train the networks using the Adam [11] optimizer with a learning rate of 10^{-3} . We perform one SGD step per environmental step. The entropy temperature α of SAC is initialized at 10^{-2} . The target entropy is -5 . The discount factor is $\gamma = 0.99$. We use a target network for the critic network and soft target update with $\tau = 10^{-2}$. The replay buffer has a capacity of 100,000 transitions. The mini-batch size is 64.

E. Baseline Details

The FERM [32] baselines use random crop for data augmentation. The random crop crops a 142×142 state image to the size of 128×128 . As in [32], the contrastive encoder has an output size of 50, and the contrastive encoder is pre-trained for 1.6k steps using the expert data. Figure 20 shows the network architecture for our baseline FERM.

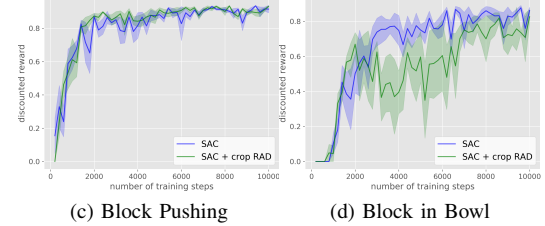
F. Action Space Choice

We perform an experiment evaluating the performance of Equivariant SAC in different action spaces in simulation. We consider the following different action spaces: 1) $dpos=0.03, drot=0.125\pi$: $x, y, z \in [-0.03m, 0.03m]; \theta \in [-\frac{\pi}{8}, \frac{\pi}{8}]$. 2) $dpos=0.05, drot=0.125\pi$: $x, y, z \in [-0.05m, 0.05m]; \theta \in [-\frac{\pi}{8}, \frac{\pi}{8}]$. 3) $dpos=0.05, drot=0.25\pi$: $x, y, z \in [-0.05m, 0.05m]; \theta \in [-\frac{\pi}{4}, \frac{\pi}{4}]$. 4) $dpos=0.1, drot=0.25\pi$: $x, y, z \in [-0.1m, 0.1m]; \theta \in [-\frac{\pi}{4}, \frac{\pi}{4}]$. In all variations, $\lambda \in [0, 1]$ stays the same. Figure 17 shows the result. The best performing action spaces are $dpos=0.05, drot=0.25\pi$ (blue) and $dpos=0.1, drot=0.25\pi$ (purple), while $dpos=0.05, drot=0.25\pi$ is more stable.



(a) Block Picking

(b) Clutter Grasping



(c) Block Pushing

(d) Block in Bowl

Fig. 18. Comparison of Equivariant SAC equipped with random crop data augmentation using RAD. The plots show the performance of the behavior policy in terms of the discounted reward. Each point is the average discounted reward in the previous 200 steps. Results are averaged over four runs. Shading denotes standard error.

$drot=0.25\pi$: $x, y, z \in [-0.05m, 0.05m]; \theta \in [-\frac{\pi}{4}, \frac{\pi}{4}]$. 4) $dpos=0.1, drot=0.25\pi$: $x, y, z \in [-0.1m, 0.1m]; \theta \in [-\frac{\pi}{4}, \frac{\pi}{4}]$. In all variations, $\lambda \in [0, 1]$ stays the same. Figure 17 shows the result. The best performing action spaces are $dpos=0.05, drot=0.25\pi$ (blue) and $dpos=0.1, drot=0.25\pi$ (purple), while $dpos=0.05, drot=0.25\pi$ is more stable.

G. Crop RAD

In this experiment, we evaluate the original version of RAD (with a random crop augmentation operator) in combination with the Equivariant SAC. We consider two variations: 1) SAC: Equivariant SAC with the default setting. 2) SAC + crop RAD: Equivariant SAC with RAD with a random crop augmentation operator. Figure 18 shows the result. In easier tasks (Block Picking and Block Pushing), SAC + crop RAD (green) shows a marginal improvement over SAC. However, SAC + crop RAD underperforms the version without RAD in the other two harder tasks. We hypothesize that this mismatched performance is because random crop augmentation, which causes a translation in the input image, will damage the rotational equivariance that the equivariant network encodes.

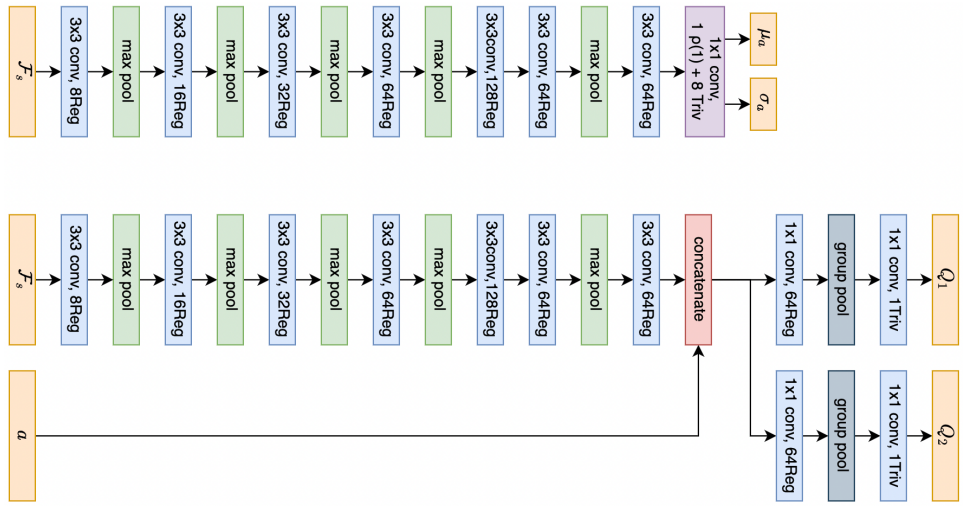


Fig. 19. The network architecture of Equivariant SAC. Top: the architecture of the actor network. Bottom: the architecture of the critic network. ReLU non-linearity is omitted in the figure.

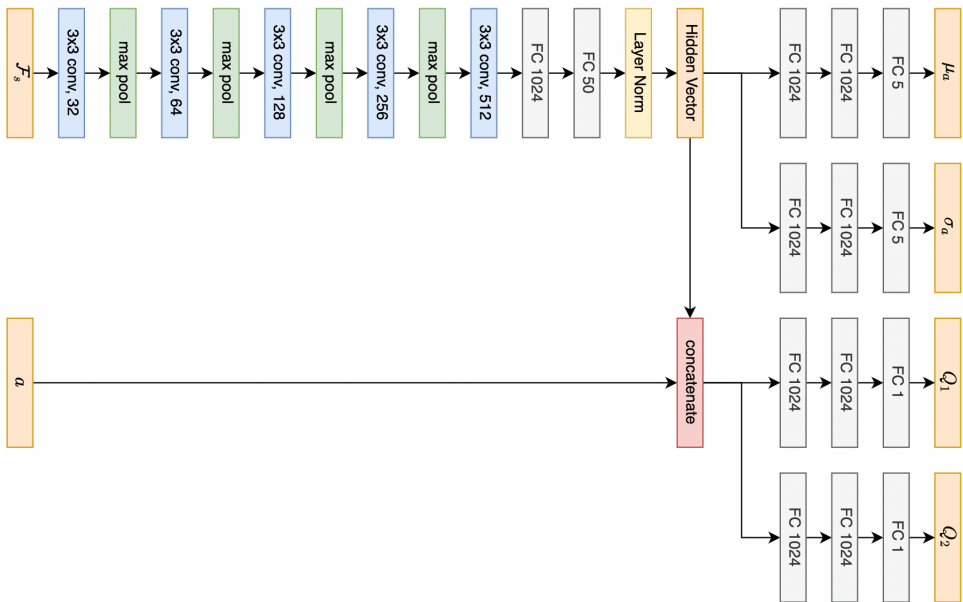


Fig. 20. The network architecture of the FERM baseline. ReLU non-linearity is omitted in the figure.